Damage caused to interlayer coupling of magnetic multilayers by residual gases

C. H. Marrows* and B. J. Hickey
Department of Physics and Astronomy, E. C. Stoner Laboratory, University of Leeds, Leeds LS2 9JT, United Kingdom

M. Herrmann, S. McVitie, and J. N. Chapman
Department of Physics and Astronomy, University of Glasgow, Glasgow G12 8QQ, United Kingdom

M. Ormston and A. K. Petford-Long
Department of Materials, University of Oxford, Parks Road, Oxford OX1 3PH, United Kingdom

T. P. A. Hase and B. K. Tanner
Department of Physics, University of Durham, South Road, Durham DH1 3LE, United Kingdom
(Received 18 August 1999)

The oscillatory interlayer indirect exchange coupling in Co/Cu multilayers is known to be highly sensitive to structural defects. In this paper the dependence of the antiferromagnetic exchange coupling on the background pressure in the vacuum chamber is investigated. Co/Cu multilayers were grown by dc magnetron sputtering in a system equipped with a leak valve to allow the introduction of low levels of air or O_2. Below a relatively narrow band of pressure the samples exhibit excellent antiferromagnetic coupling and consequently a high giant magnetoresistance, $\sim 40\%$ for $\{Co(8\ Å)/Cu(8\ Å)\}\times 25$ samples. Above this transitional band of pressure no antiferromagnetic coupling, and hence no giant magnetoresistance, is observed. X-ray diffraction measurements reveal no change of any significance in any of the layer thicknesses or roughnesses. Whilst the high-field magnetic behavior is found to be isotropic in the sample plane, the reversal of the remanent moment around zero field is found to show a varying degree of uniaxial anisotropy. Lower remanent moments are found to be associated with a more isotropic reversal mechanism. A thorough characterization of the physical and magnetic microstructure by means of various modes of transmission electron microscopy is presented. Cross-sectional images reveal subtle changes in the crystallinity and layer quality of the samples as the background pressure is increased. Plan-view Lorentz microscopy reveals that the isotropic reversal mechanism of the low remanence samples involves a complete domain structure. The reversal mechanism of multilayers with a significant remanent moment varies markedly with field direction and can be dominated by rotation or comparatively simple domain processes. Samples with a significant giant magnetoresistance $\sim 20\%$ and remanent fractions ~ 0.7 are found to still show highly anisotropic reversal mechanisms around zero field. Indeed when demagnetized along the easy axis the samples are in a single domain state at remanence. This is compelling evidence for substantial noncollinear ordering of the moments through biquadratic coupling.

I. INTRODUCTION

One of the most striking properties of the new generation of artificial magnetic multilayer materials is the oscillatory indirect exchange coupling between two magnetic films separated by a thin nonmagnetic spacer.[1] For those thicknesses of spacer layer where the coupling is antiferromagnetic, the application of a magnetic field to such an artificial antiferromagnet can cause the system to undergo a metamagnetic transition. The associated drop in electrical resistivity as the magnetic configuration changes from antiferromagnetic (AF) to ferromagnetic (FM) is termed the giant magnetoresistance (GMR).[2] As the layer thicknesses in such samples are on the nanometer scale, the preparation techniques for such materials are exacting and few structural defects can be tolerated. In general the consensus is that the best quality structures are prepared under ultrahigh vacuum (UHV) conditions, although there have been few attempts to quantify the effects of background gases on the GMR and coupling of such materials. There is broad agreement that H_2O and O_2 are particularly damaging.[3,4] Other authors find a more complex behavior, with the suggestion that certain low levels of O_2 can be beneficial, at least in spin-valve structures where the interlayer coupling is not necessary to observe GMR.[5]

We have shown previously that a high level of cleanliness is necessary for a high GMR in Co/Cu multilayers, as residual gases damage the film in such a way as to reduce the antiferromagnetic coupling.[6] Moreover, by selectively damaging only certain parts of the sample with gas, we found that the part of the multilayer most susceptible to damage is the bulk of the Cu spacer. This was accomplished by pausing growth at a certain point in the multilayer stack and allowing residual gases from the chamber to adsorb onto the film surface. Multilayers where the spacers are only lightly damaged may still show appreciable GMR, although the remanence may be considerable. The GMR ratio was always found to be higher than would be dictated by a simple series circuit of AF and FM coupled regions in the proportions stipulated by the remanent fraction. In fact the GMR ratio is found to have a parabolic dependence on the remanent fraction, suggesting the possibility of noncollinear arrangements of adjacent layer moments at zero field.[7] Such noncollinear arrangements of

layer moments have been observed in a large number of layered magnetic systems, and can be explained by the introduction of a non-Heisenberg biquadratic term into the indirect exchange energy. This is to be compared with the alternative explanation of the nonzero remanance in poorly AF-coupled multilayers, where ferromagnetic bridges, or pinholes in the spacer layers, are said to lead to a ferromagnetically coupled volume fraction.[8] This would lead to a domain structure at zero field, containing low-total-moment (AF-coupled) and high-total-moment (FM-coupled) regions.

Biquadratic interactions in multilayered systems continue to attract much experimental and theoretical attention. Almost all investigated coupled multilayer systems have been found to exhibit some degree of biquadratic coupling. Recently studied examples include Fe/Cr,[9,10] Co/Au,[11] Co/Ir,[12] as well as systems with semiconducting (Fe/Si) (Ref. 13) and insulating (e.g., Co/Al-O/NiFe) (Ref. 14) spacer layers. Many more can be found in a recent review by Demokritov.[15]

The aims of the work reported in this article were twofold: to determine unambiguously the zero-field moment configuration of a sample showing reduced GMR, and to attempt to find evidence for the residual gas damage in the physical microstructure. Towards these goals we employed various modes of transmission electron microscopy (TEM) to image both the physical and magnetic microstructures of samples showing different interlayer coupling, and consequently differing GMR ratios.

Sequences of samples were grown on both ordinary Si substrates and Si_3N_4 window substrates that are suitable for plan-view TEM imaging. By application of different imaging modes it was possible to investigate the physical and magnetic microstructure of the samples without any further preparation. The layered structure of the sample was examined by cross-sectional transmission electron microscopy (XTEM), imaging vertical slices of the samples grown on Si. As the base pressure of the growth chamber was raised a reduction in both GMR ratio and AF coupling could be observed. These may be linked to changes in the low-field reversal modes of the remanent moment, observed both magnetometrically, and by micromagnetic imaging. In the following section of this paper we will describe the various experimental techniques used. We will then present the magnetotransport and magnetometric data for the samples, followed by the various electron micrographs. In the final section we shall draw some conclusions.

II. SAMPLE PREPARATION AND EXPERIMENTAL TECHNIQUES

Samples were deposited by dc magnetron sputtering in a custom-built vacuum system at the University of Leeds. The system is equipped with six sputtering targets and has a base pressure of better than 2×10^{-8} Torr. This is achieved by a combination of cryopumping to $\sim1\times10^{-7}$ Torr, followed by the filling of a Meissner trap.[16] This is particularly effective in the pumping of water, the main residual gas remaining after cryopumping. The residual gas composition was determined using a quadrupole mass spectrometer. Once the trap is filled the residual gas is mainly comprised of N_2 or CO (mass peak 28). In order to control accurately the level of background gas damaging the film, air or O_2 was introduced through a fine leak valve. The working pressure of 99.9999% purity Ar was 3.0 mTorr, introduced through an ultrahigh vacuum compatible stainless steel line. Typical deposition rates were 2.6 Å/s for Co and 2.9 Å/s for Cu. A magnetic field of 200 Oe was applied in the substrate plane during growth of the whole multilayer stack by a permanent magnet array inside the chamber. To minimize uncontrolled changes in deposition conditions, groups of samples that are directly compared were deposited in a single growth run.

All the samples discussed in this paper are of the form {Co(8 Å)/Cu(8 Å)}×25. The Cu thickness was selected to match the first AF-coupling peak in the oscillation. No buffers or caps were used as we have found these to be unnecessary for good quality growth and sample longevity. Growth was paused for 10 s in the middle of every Cu spacer, to allow residual gases to sorb onto the surface.

Magnetoresistance was measured by the conventional four-probe dc technique. Magnetization loops were measured by the Magneto-Optic Kerr Effect (MOKE). The field was always applied in the plane of the sample. Low-angle x-ray scattering measurements were performed at station 2.3 at the Synchrotron Radiation Source at Daresbury Laboratory.[17] The wavelength of x rays used was 1.38 Å, close to the Cu K absorption edge. All of these measurements were performed at room temperature.

The samples grown on the window substrates were investigated at the University of Glasgow in microscopes highly modified to optimize magnetic-imaging conditions. The physical microstructure was studied using conventional (bright-field) imaging and diffraction techniques. The magnetic microstructure was investigated using the Fresnel mode of Lorentz microscopy.[18] Fresnel imaging shows domain walls as black and white lines (''wall contrast''). In polycrystalline samples the magnetic dispersion gives rise to ripple contrast which appears within domains as fine black and white lines running perpendicular to the mean direction of magnetization. The magnetizing experiments were carried out in a modified Philips CM20 TEM with a field-emission gun. In this instrument the primary imaging lenses used while investigating magnetic samples are so-called Lorentz lenses. By exiting the standard objective lens as appropriate, a magnetic field is generated that is perpendicular to the sample plane. Tilting the sample generates a well-known in-plane field component which has the magnitude $H_{\text{in-plane}} = H_{\text{objective}} \sin\alpha$, with α being the tilt angle. The highest possible field ($H_{\text{in-plane}} \approx 6\times10^3$ Oe) was applied first to the samples before the objective lens field was reduced to the value suitable for the investigation of the samples ($H_{\text{objective}} \approx 90$ Oe). Therefore while taking the magnetizing sequences the samples were only subjected to a very small vertical field.

Cross-sectional TEM images were taken at the University of Oxford. The samples were cleaved, thinned by ion-milling, and imaged. The cross-sectional high-resolution electron microscopy and bright-field images were recorded using a JEOL 4000EX operated at 400 kV (point-to-point resolution 0.16 nm). In all cases the sample was aligned so that the electron beam was parallel to the [110] direction in the Si substrate so that the interfaces between the layers could be viewed end-on.

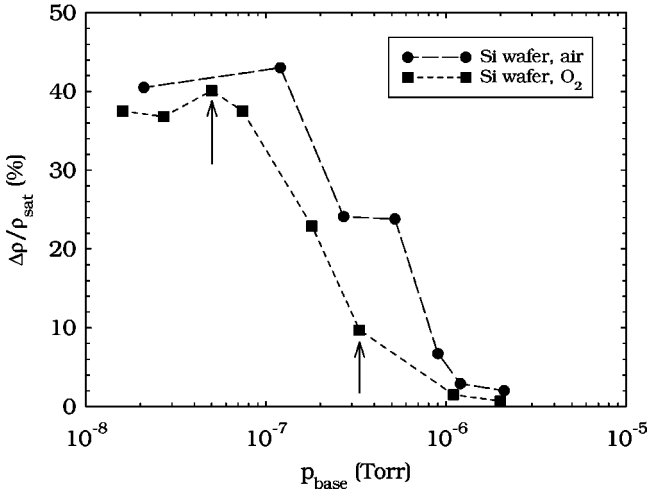

FIG. 1. The giant magnetoresistance for samples of the form {Co(8 Å)/Cu(8 Å)}×25 on (001) Si as a function of the base pressure. Deposition was paused for 10 s in the middle of every Cu spacer layer. The lowest pressure point corresponds to the lowest attainable pressure in the chamber, higher pressures correspond to the introduction of air (circles) or O_2 (squares). The samples marked with arrows are those which were imaged by XTEM. Note the logarithmic scale on the abscissa.

Samples were grown on pieces of (001) Si wafer with the native oxide layer left intact for some magnetoresistance measurements and for cross-sectional TEM imaging. For plan-view and Lorentz-imaging samples were deposited onto Si_3N_4 membranes supported on Si wafer suitable for direct observation in the TEM.[19] These samples were also studied by MOKE. Meanwhile larger pieces of nitride-coated Si wafer were used for GMR and MOKE experiments. Pairs of such samples (TEM membrane and larger piece of wafer) were mounted side by side on the substrate holders, so that the multilayers were grown simultaneously, allowing their properties to be directly compared.

III. RESULTS

In Fig. 1 we show the decrease in GMR ratio in two series of samples as the base pressure is raised by the introduction of air or oxygen through the leak valve. All these samples were grown on (001) Si wafers. For pressures below a transitional band a GMR ratio of ~40% was achieved in both series. This moderate GMR value is due to diffusive boundary scattering at the surfaces of the multilayer limiting the spin-allowed mean free path,[20] due to the small number of bilayer repeats. The expected level of impurity introduced with the working Ar is $\sim 3\times10^{-9}$ Torr, well below the pressure range on the abscissa of the graph. In the high-pressure regime above the transition zone the GMR is very low. Both series show a broad transition region, at a higher base pressure for air than for O_2 alone. The transition pressures differ by approximately a factor of three across the whole curve, not quite the 5:1 ratio one might expect if the N_2 were entirely inert. The saturated resistivities of all these samples are comparable, falling in the range 20 ± 2 $\mu\Omega$ cm. The changes in GMR are caused by a decrease in the amount of AF alignment in the samples as the pressure is raised, as borne out by an increase in remanent fraction as observed by MOKE. We can see that pure oxygen is much more damaging than air in this regard. This suggests that N_2 is much more inert than O_2, as might be expected.

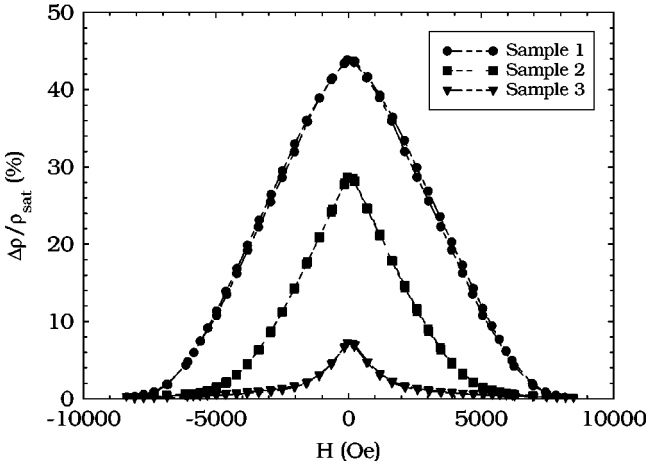

FIG. 2. Giant magnetoresistance loops for the large samples grown on Si_3N_4 at three different base pressures; Sample 1, 1.8×10^{-8} Torr (circles); Sample 2, 6.2×10^{-7} Torr (squares); and Sample 3, 0.9×10^{-6} Torr (triangles). The magnitude of the giant magnetoresistance falls as the base pressure is increased. The saturated resistivity of all three samples is close to 20 $\mu\Omega$ cm.

In Fig. 2 we show GMR loops for three samples deposited on the nitride-coated Si wafer at different chamber background pressures. As O_2 is introduced into the chamber a drop in GMR ratio is again observed. As these three samples will be extensively discussed we shall refer to them as samples 1, 2, and 3. These multilayers are comparable to similar samples grown directly onto the Si wafer, as the nitride surface is similarly smooth. It can also be seen in this figure that the shape of the loop is changing. With the leak valve closed (1.8×10^{-8} Torr) the GMR peak has a convex top, close to the parabolic GMR response of an ideally AF-coupled multilayer (sample 1). As the pressure rises to 6.2×10^{-7} Torr the field required to saturate the samples falls and the GMR peak becomes more pointed (sample 2). These effects are greater still as the pressure is finally raised to 0.9×10^{-6} Torr (sample 3). Again the sample resistivities are all comparable in the magnetically saturated state, with values of about 20 $\mu\Omega$ cm. They are, of course, different at zero field due to the different magnetoresistance ratios. Such changes in GMR loop shape are associated with biquadratic coupling.[21]

Grazing incidence specular x-ray scans for these three samples are presented in Fig. 3. The data represent the true specular scatter, determined by subtracting the diffuse scatter measured in another scan with the sample offset from the specular condition by a small amount from the scan measured along the specular ridge. The three samples are very similar, in each case there being well-defined Kiessig fringes, and a similar rate of intensity fall-off with increasing sample angle. This indicates that the roughness in the samples is low, and of very similar amplitude. The first-order superlattice Bragg peaks are of similar intensity and full width half height maximum. The Bragg peaks are not all at the same angle, representing bilayer periods of 16.1 Å, 15.2 Å, and 16.4 Å in order of increasing background pressure (samples 1, 2, and 3). This represents a sample-to-sample fluctuation

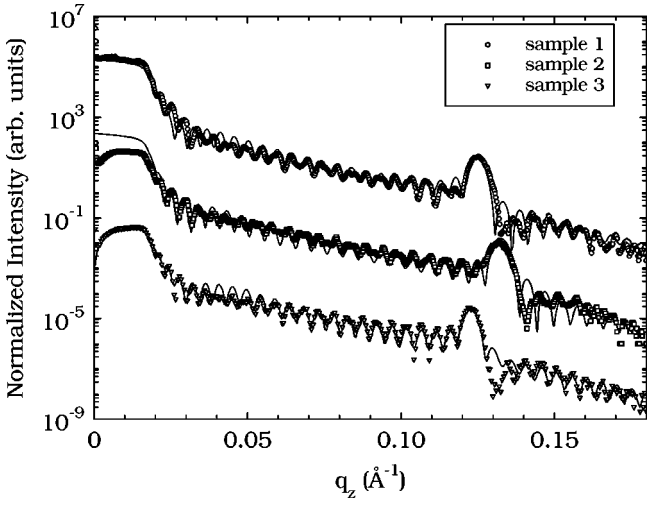

FIG. 3. Low-angle x-ray specular reflectivity scans for the three samples grown on Si_3N_4. Sequential curves have been offset by decades of intensity for clarity. There are no significant differences between the profiles. The Bragg peak positions correspond to bilayer periods of 16.1 Å, 15.2 Å, and 16.4 Å. The solid lines are simulated fits to the data.

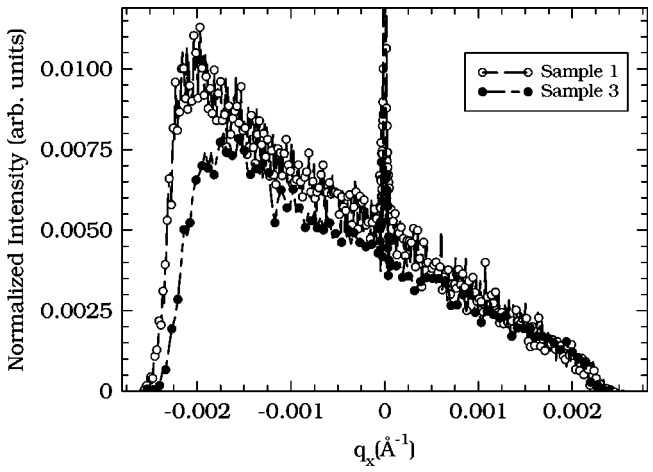

FIG. 4. Transverse diffuse x-ray scans for the extreme samples 1 (open points) and 3 (solid points). The remarkable similarity in both intensity and distribution of scatter indicates that the Co/Cu interface structure is almost identical. The slight difference between the two scans to the left of the figure originate from unequal sample sizes.

of better than 1 Å from the nominal period of 16 Å. The data have been modeled using the Bede Scientific REFS MERCURY code to determine individual layer thickness and roughness parameters. Simulated curves are included in Fig. 3. The rms roughness of all the layers in the samples is ~5.5 Å. From the model simulation we have also determined that the fluctuations in the Co layer thickness from sample to sample are much greater than those in the Cu spacer layer. It follows that the changes seen in the GMR in Fig. 2 cannot be explained by incorrect spacer thickness—a result corroborated by the fact that the AF-coupling peak width and position are not affected by this type of residual gas damage.[7]

Transverse diffuse scans (specimen scan at constant scattering angle) taken through the first-order superlattice Bragg peak showed a very similar intensity ratio between the integrated diffuse scatter I_d and the integrated specular scatter I_s (Fig. 4). Using the Born wave approximation, we find that the conformal roughness on the Co/Cu interfaces is ~2.5 Å for all samples. The overall distribution of the diffuse scatter with angle is also very similar for all three samples, indicating that the in-plane correlation length is the same. We could find no differences in the interface structure between any of the three samples. A more detailed account of the characterization of similar Co/Cu multilayers by x-ray diffraction has been published elsewhere.[22]

The changes in GMR amplitude despite the absence of difference in the saturated resistivity is suggestive of a reduction in AF coupling. This would not affect the saturated resistivity, as the samples are in the same magnetic state with all the layer moments aligned parallel to the field. On the other hand, the resistivity enhancement at zero field will be much smaller than anticipated if the degree of antiparallel alignment is not high. This is borne out by MOKE loops for the samples, shown in Fig. 5. The drop in magnetoresistance can be explicitly linked with the rise in remanent fraction, as in a previous study.[7]

Two loops are presented for each sample, measured with the field applied along the growth field direction and perpendicular to it. We note that the shapes of these loops are isotropic in field direction. This is to be expected as any anisotropy induced in Co by the growth field is generally found to be weak,[23] while the field required to overcome the coupling is much larger, of the order of a few kOe. However in the low-field MOKE loops presented in Fig. 6 we can see that some anisotropy is present as the remanent moment reverses. For convenience we shall refer to the direction parallel to the growth field as the easy axis, and perpendicular to it as the hard axis. As we shall see, although the degree of anisotropy varies from sample to sample, the ''easiest'' direction is always defined by the growth field.

In Fig. 6(a) we see that both the easy and hard axis loops for sample 1 show considerable rounding. There is some weak anisotropy although the coercivity is 27 Oe in both easy and hard directions. Both loops are somewhat canted. Meanwhile, Figs. 6(b) and 6(c) are quite similar, with a squarer easy-axis loop and a canted, lower hysteresis hard-axis loop. The coercive fields are 38 Oe (easy axis) and 35 Oe (hard axis) for sample 2 and 31 Oe (easy axis) and 20 Oe (hard axis) for the slightly more anisotropic sample 3. At first, it is tempting to link the degree of induced anisotropy in the films with the exposure to oxygen, and there have been attempts to do this in the past.[24,25] However, we have found that the correlation is between the degree of anisotropy and the remanence. For example, samples grown with 15-Å Cu spacers, corresponding to the second FM peak, are always highly anisotropic in their reversal mechanism, regardless of the degree of exposure to O_2 or any other background gas. For samples with a very low remanence due to excellent AF coupling the anisotropy at low fields can be very small.[26]

In order to gain a more detailed insight into the reversal mechanisms of the samples, magnetizing experiments were carried out, in which the magnetic microstructure was monitored constantly using the Fresnel mode of Lorentz microscopy. For all investigated samples it was found that the magnetization reversal processes were dependent on the direction of the in-plane component of the applied field. By applying

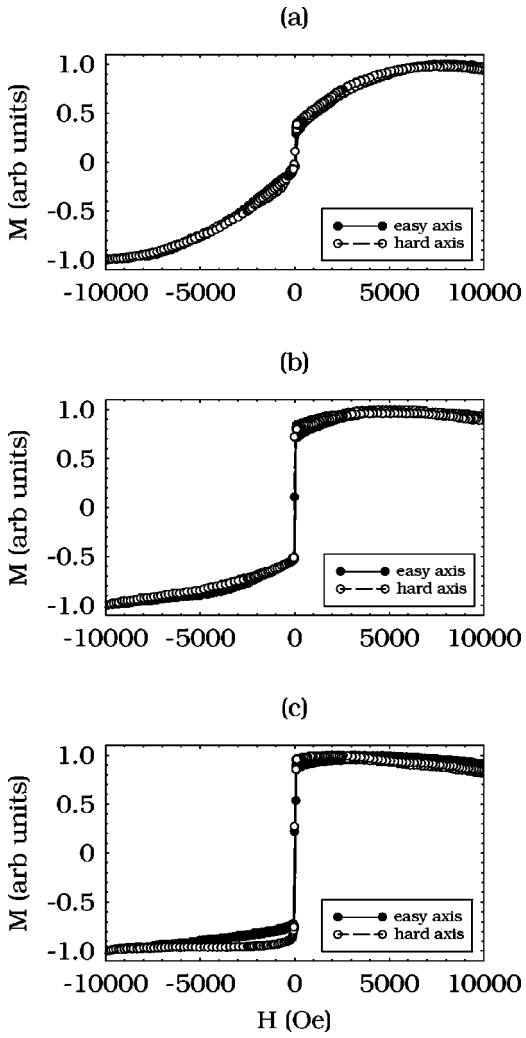

FIG. 5. High-field MOKE loops for the three large samples grown on Si_3N_4. The remanence rises as the GMR falls. The loops were measured with the field applied along the growth field direction (solid points) and perpendicular to it (open points). All three samples were found to be isotropic on this scale. (a) Base pressure $=1.8\times10^{-8}$ Torr (Sample 1); (b) 6.2×10^{-7} Torr (Sample 2); (c) 0.9×10^{-6} Torr (Sample 3).

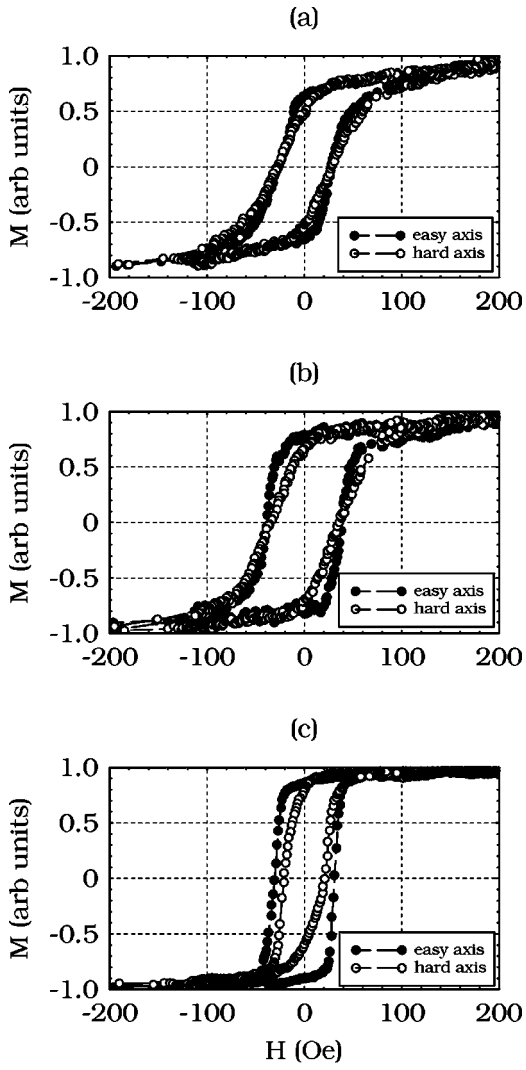

FIG. 6. Low-field MOKE loops for the three samples shown in Fig. 5. Again, solid points are for loops measured with the field applied along the growth field direction, and open points for those with the field perpendicular to it. A varying degree of anisotropy is exhibited, with greater anisotropy associated with a higher remanent fraction. (a) Base pressure $= 1.8\times10^{-8}$ Torr; (b) 6.2×10^{-7} Torr; (c) 0.9×10^{-6} Torr. Note that the units of magnetization are not the same as those for the same sample shown in Fig. 5.

fields *in situ* with the specimen in different orientations the hard axis was identified. Application of a field in this direction led to the formation of low-angle walls and magnetization rotation within these domains. Wall movement was present in all investigated samples and a very common feature is the formation of 360° walls. Extracts of the reversal processes of the samples with the field in the orthogonal direction are shown in Figs. 7, 8, and 9. Although this is what was called the easy axis in the discussion of the MOKE loops, what is observed does not clearly resemble an easy-axis process in a simple magnetic film. There is a pair of images shown for each sample, one of which is taken at remanence (sample untilted in the vertical field). As the micromagnetic behavior differs most markedly for sample 3, we will begin by discussing this sample.

At remanence considerable magnetic dispersion is present although the clear directionality of the magnetization ripple indicates that the mean direction of magnetization lies parallel to the direction in which the field had been applied (Fig. 7). Field reversal leads first to an increase of dispersion and the development of low-angle domain walls. At higher fields there is rotation of the magnetization in adjacent domains indicated by an increase in wall contrast. However, significant reversal of magnetization does not occur until a field of -30 Oe when a large domain is generated with the walls almost perpendicular to the array of walls developed at lower fields and still clearly visible in the areas marked *P* and *Q* in Fig. 7. The newly formed domain was observed to expand in the center of the field of view without any further increase of the applied field showing the importance of time-dependent effects in this regime. The overall behavior is consistent with the squarish low-field MOKE loop. It should be noted that the domain walls (*A* and *B*) are very irregular but that the degree of dispersion within the reversed region is quite similar to that observed over the whole field of view at remanence. Hence the mean direction of magnetization can once

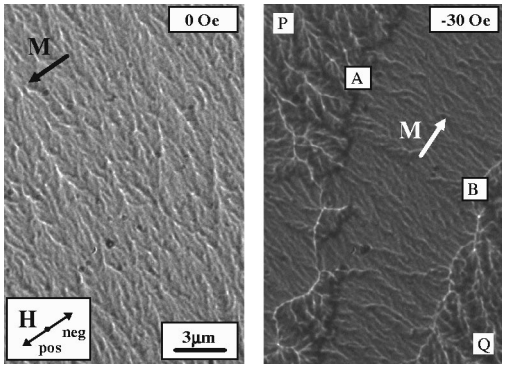

FIG. 7. Fresnel images of sample 3; field direction ⊥ hard-axis-like direction, field values given, mean direction of magnetization as indicated, *A* and *B* denote domain walls.

again be deduced as indicated in Fig. 7. Further increase of the reverse field to −44 Oe results in an almost single domain state of the sample. Samples 2 and 1 also show directionality of the magnetic dispersion in the remanent state with the mean direction of magnetization being parallel to the applied field (Figs. 8 and 9). It was, however, not possible to determine a direction of magnetization that leads to the sharp switch in magnetization of sample 2 corresponding to the low-field MOKE loop of this sample. Instead, samples 2 and 1 look much more alike in these TEM experiments with their magnetization-reversal processes being in better agreement with the kind of hysteresis loop of sample 1, where the magnetization reversal in the easy-axis-like direction is more gradual. In both of these samples we observe the formation of highly complex domain structures without dominant directionality.

The differences in magnetic contrast for the different samples is consistent with their GMR values. Good antiferromagnetic alignment results in high GMR and little magnetic contrast. Perfect antiferromagnetic alignment in alternate layers would result in no overall Lorentz deflection of the electron beam while passing through the layer stack. Therefore the high contrast of sample 3 is in agreement with the low GMR of this sample (~7%), whereas the much lower contrast of sample 1 is consistent with better antiferromagnetic alignment and higher GMR (~44%). It is possible to identify all the switching behavior observed in the TEM with the coercive fields measured from the low-field MOKE in Fig. 6.

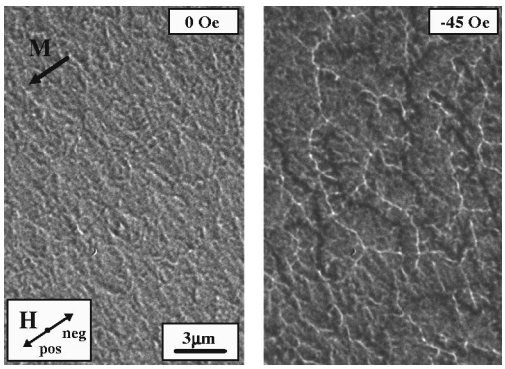

FIG. 8. Fresnel images of sample 2; field direction ⊥ hard-axis-like direction, field values given, mean direction of magnetization as indicated.

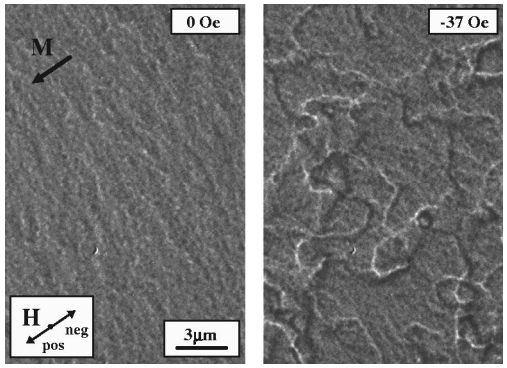

FIG. 9. Fresnel images of sample 1; field direction ⊥ hard-axis-like direction, field values given, mean direction of magnetization as indicated.

The plan-view bright-field images of all investigated samples are indistinguishable. An example is shown in Fig. 10. The samples are of micropolycrystalline structure with an average grain size in the range of 15–20 nm with no texture present as can be seen in the diffraction pattern of the tilted sample (Fig. 10). The majority of the crystallites have fcc structure, but there is evidence for a fraction of hcp crystallites from the diffraction patterns.

As we have previously reported,[6,26] we have been unable to find any differences in the physical microstrucure between clean AF-coupled samples, and those so heavily damaged by residual gases as to be entirely FM coupled. Techniques used include synchrotron x-ray analysis, ^{59}Co nuclear magnetic resonance,[6] and plan-view TEM (Ref. 26 and this work, Fig. 10). All these findings are consistent with those reported here.

Figure 11 shows in-focus high-resolution XTEM images of the two samples marked in Fig. 1. On the far left of the images the highly ordered crystalline Si substrate can be seen, with a thin (~15 Å) amorphous native oxide layer visible as a bright band between it and the sample. Epoxy

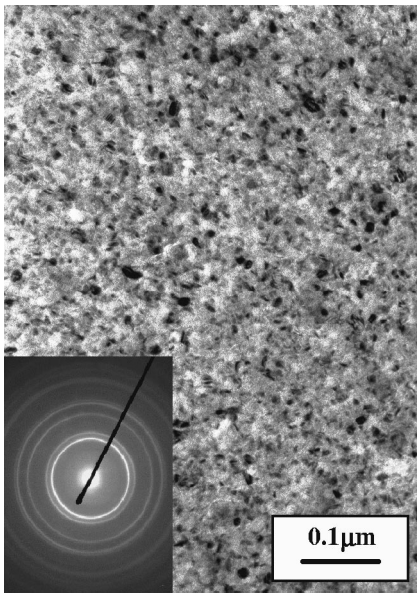

FIG. 10. Plan-view bright-field image of sample 2; inset shows diffraction pattern of tilted sample.

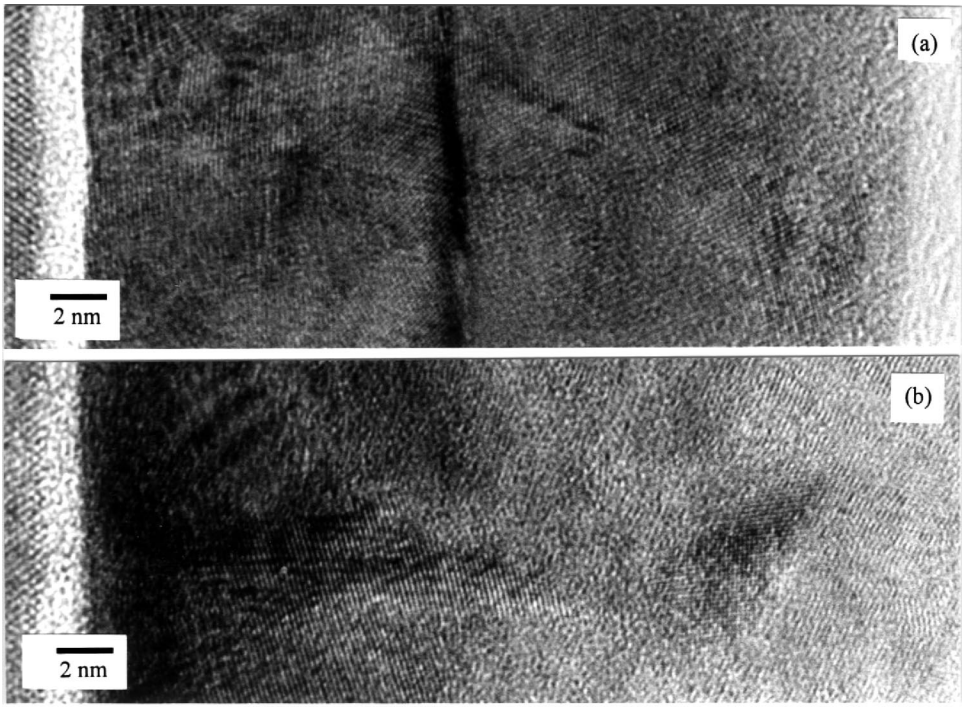

FIG. 11. In focus high-resolution XTEM images for two samples of the form {Co(8 Å)/Cu(8 Å)}×25 grown on (001) Si wafer. The Si is visible on the left of the micrographs as a highly ordered crystalline layer. Next to this is the native SiO_x layer, which is seen to be amorphous. The contrast between individual Co and Cu layers is not visible in this image due the close proximity of these two elements to each other in the Periodic Table.

used in sample mounting can be seen at the right of each image. The contrast between Co and Cu atoms is poor due to their close proximity in the Periodic Table. As a result the layered structure of the samples is not evident in these images. We can see that the samples consist of columnar grains. In the low-background-pressure sample [Fig. 11(a)] the grains extend throughout the height of the entire multilayer film in places. This does not always appear to be true in the high-background-pressure sample [Fig. 11(b)]. Some strain is evident. Most of the fringes visible in the film are the (111) fringes of the fcc Co or Cu structure. The lack of texture is evident, with {111} planes making a wide variety of angles with the film normal. In certain areas of the images overlapping grains give rise to Moiré fringes. The crystal structure seen in the image of the higher-background-pressure sample is slightly less good, but even in the cleaner sample the degree of crystallographic perfection is not at all high.

For the correct level of defocus the chemical periodicity of the multilayer is seen, as shown in Fig. 12. These images are best viewed at a shallow angle looking along the layers. We can see that for the first few bilayers the layering structure is poor, resulting in a ferromagnetic block of CoCu alloy. This is consistent with the lack of GMR in multilayers with very low numbers of bilayer repeats ($N \lesssim 5$),[20] and with the results of fitting polarized neutron reflectivity spectra for such samples.[27] It must also account for at least some of the remanence observed in MOKE loops, such as Fig. 5(a), although that is a different sample to that imaged in Fig. 12(b). The lighter bands are the Cu spacer layers. For the low-background-pressure sample the layers are mostly continuous, if somewhat wavy in places. In the higher-background-pressure samples the layers show a few more discontinuities, with a small number of ferromagnetic bridges across the Cu present. Although the differences are very subtle, these XTEM images represent the only observed differences in the physical microstructure of such samples to date. This statement carries with it the caveat that it would prove impossible to infer the level of background gas that a sample had been exposed to only from XTEM images of this sort.

IV. DISCUSSION AND CONCLUSIONS

The rise in remanence and reduction in GMR in samples which are gas damaged clearly indicate that the AF ordering is far from perfect. The presence of GMR in these samples means that some degree of nonparallel alignment exists between the moments at zero field however, and this can be quantified by the remanence displayed by the samples in Fig. 5. If we wish to describe the smooth transition from AF to FM coupling with increasing base pressure by simply increasing the FM-coupled volume fraction then we should expect to see regions in the Lorentz images with very different contrast, corresponding to variations in the resultant magnetic moment. In fact, the images reveal overall uniform contrast in all three samples, moreover in the wide anhysteretic regimes from about 50 Oe to saturation the samples are single domain. It is possible to explain this apparent contradiction by the introduction of the possibility of noncollinear ordering, as suggested by previous results.[7] This would allow the angle between the moments to vary smoothly from π to 0 as the base pressure in the sputtering system crosses the transition zone.

Suppose the moments in a Co/Cu/Co trilayer take angles θ_1 and θ_2 with respect to an applied field H. We may write the energy per unit area of such a trilayer as

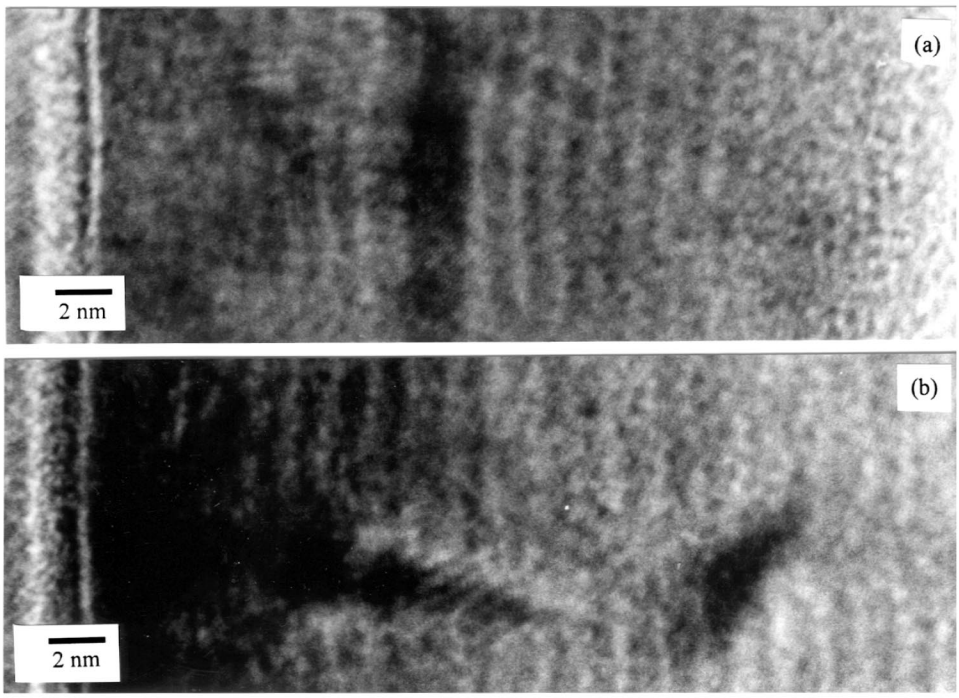

FIG. 12. Out-of-focus high-resolution XTEM images of the same areas as displayed in Fig. 11. In these images the layer structure is visible, while the defocus is such that the individual atoms can no longer be discerned. The lighter bands are the Cu layers.

$$\epsilon = -\mu_0 t_{\mathrm{Co}} MH(\cos\theta_1 + \cos\theta_2) - J_1\cos(\theta_1 - \theta_2) - J_2\cos^2(\theta_1 - \theta_2), \quad (1)$$

where the Co layers are of magnetization M and thickness t_{Co}. The coupling is parameterized by two constants J_1 and J_2, which are the bilinear and biquadratic coupling energies, respectively. It is the presence of a substantial biquadratic term that leads to noncollinear ordering of the moments at low fields. To transfer this model to a multilayer we have only to note that each layer will be coupled to two neighbors, and adjust the coupling constants by an appropriate factor of 2.

It is possible to determine the coupling constants and equilibrium angles from fitting the high-field MOKE and GMR curves by numerically following the path of minimum energy in Eq. (1) as H is varied. As an alternative in simple systems, some features may be determined analytically. Setting $\Theta = \theta_1 - \theta_2$ and setting partial derivatives $\partial\epsilon/\partial\theta_1 = 0$ and $\partial\epsilon/\partial\theta_2 = 0$ to find the angles of minimum energy, we find that

$$H_{\mathrm{sat}} = -\frac{4(J_1 + 2J_2)}{\mu_0 M t}, \quad (2)$$

$$\Theta_0 = \cos^{-1}\frac{-J_1}{2J_2}. \quad (3)$$

The remanant fraction may be determined directly from Eq. (3) as $\cos(\Theta_0/2)$. Measurement of the remanent fraction and saturation field hence leads directly to a determination of the coupling constants J_1 and J_2 and the equilibrium angle between the moments Θ. These results are presented for our three samples in Table I, assuming $M = 1.0$ MA m^{-1} and $t_{\mathrm{Co}} = 8$ Å. We have used this value for M, which is significantly below the bulk value (1.422 MA m^{-1}), as we have found previously that there is significant reduction in moment in very thin Co layers at finite temperature.[28] Recent vibrating sample magnetometer measurements[29] on these samples confirm that this is a reasonable value.

We have argued that the samples have a uniform resultant magnetic moment horizontally from the uniformity of contrast observed in the Lorentz TEM. Since these images represent an integration of the magnetic moment of the sample in the vertical direction they are not directly sensitive to vertical inhomogeneities. We do have evidence to suggest that the samples are magnetically uniform in the vertical direction apart from the small number of FM-coupled layers near to the substrate. Some information can be deduced from the Lorentz images themselves, in particular around the domain walls. Only on rare occasions is any splitting of the walls visible, meaning that the walls are coherent throughout the height of the stack. Moreover, in recent polarized neutron reflectometry measurements the vertical coherence length of the magnetic scatter was always found to be the full height of the multilayer stack, even in much more weakly coupled 2nd AF peak Co/Cu samples.[30] Finally, the effects we describe in the present article have been found to be independent of the number of bilayer repeats deposited. The dependence of

TABLE I. The parameters determined for the three samples subjected to magnetic analysis.

	J_1 (mJ m^{-2})	J_2 (mJ m^{-2})	Θ_0
Sample 1	−0.064	−0.035	156°
Sample 2	−0.013	−0.038	100°
Sample 3	0.033	−0.036	60°

GMR and remanence on base pressure has been found to be the same for multilayers with 10, 25, and 50 bilayer repeats. We therefore believe that the degree of uniformity of the resultant magnetic moment is high in both the vertical and horizontal directions.

The Lorentz TEM studies of the low-field reversal mechanisms reveal some anisotropy in all three samples, as borne out by the low-field MOKE. In all three cases the easy axis was defined by the growth field direction in the sputtering chamber. However, the degree of anisotropy seems to be related to the quality of the AF coupling, with good AF samples showing a more isotropic response to the applied field. In the Lorentz TEM, it was not possible to find an obvious easy axis in samples 1 and 2 where the magnetization switches sharply. The details of why a sample with a larger remanent moment should show a more pronounced anisotropy are unclear at this stage. Another interesting feature of these experiments is that samples 2 and 3 seem more similar in the low-field MOKE, while in the Lorentz images samples 1 and 2 are more alike. It should be noted however that the samples all exhibit a continuous rise in GMR, AF alignment, and isotropy of reversal with falling base pressure during deposition. Sample 2 simply appears more like 1 or 3, depending on the measurement technique used.

The XTEM images appear to show the presence of regions where there are discontinuities in the Co and Cu layers, and there are more such regions in the gas-damaged sample. However, the presence of pinholes is not disastrous for the noncollinear model. The work of Bobo shows significant twisting of the moments around a pinhole, leading to substantial noncollinear ordering over a large area of film.[31,32] If the pinholes are sufficiently close together laterally then the preferred interlayer angle is ''averaged'' over the area of the film.[33] In NiFe/Cu, a substantial J_2 (and the anomalous change in sign of J_1 with temperature) were directly attributed to the presence of pinholes.[34] First AF peak Co/Cu multilayers from another deposition system with comparatively large remanence have also been recently found to exhibit dominant biquadratic coupling.[35]

A brief remark on the growth of similar films by molecular-beam epitaxy (MBE) is in order at this point: the work of Miranda suggests that the presence of pinholes is a characteristic feature of the growth of (111) Co/Cu by this technique,[36] unless suppressed by the use of surfactants. This is due to the possibility of twinned growth domains forming in this system, giving rise to relatively open grain boundaries when they meet. Because of this problem there has been some controversy over whether[37] or not[38] it is possible to obtain any AF coupling in Co/Cu multilayers grown by this technique. On the other hand, there have been many reports of near-perfect AF coupling and very high GMR in sputtered Co/Cu layers of many different textures, including (111).[39] Reasons for this are not clear—sputtering is a much more energetic process, and it has been shown that heavily reflected neutral bombardment can be correlated with dense compressive grain boundaries and high GMR.[40] It may be that impurities in the Cu change the surface energies sufficiently to maintain the structural imperfections that give rise to the pinholes during the sputtering process. For the purposes of this article it seems wise to terminate this line of speculation at this point.

To summarize, we have observed a monotonic decrease in GMR and increase in remanence in Co(8 Å)/Cu(8 Å) multilayers as the base pressure of the sputtering chamber in which they were prepared rises. To explain these changes consistently with magnetizing sequences of Lorentz TEM images, we must invoke a substantial biquadratic term in the exchange coupling between neighboring Co layers. This results in configurations of the moments that are not collinear.

ACKNOWLEDGMENTS

C.H.M. was supported by the Royal Commission for the Exhibition of 1851. The work of M.H. was supported by a TMR grant of the European Commission. A.K.P.-L. was supported by the Royal Society. We would also like to thank the Engineering and Physical Sciences Research Council for funding.

*Electronic address: c.marrows@leeds.ac.uk

[1] *Ultrathin Magnetic Structures*, edited by B. Heinrich and J. A. C. Bland (Springer, Berlin, 1994), Vol. 2, Chap. 2.
[2] B. Dieny, J. Magn. Magn. Mater. **136**, 335 (1994).
[3] F. Yoshizaki and T. Kingetsu, Thin Solid Films **239**, 229 (1994).
[4] K. Kagawa, H. Kano, A. Okabe, A. Suzuki, and K. Hayashi, J. Appl. Phys. **75**, 6540 (1994).
[5] W. F. Egelhoff, P. J. Chen, C. J. Powell, M. D. Stiles, R. D. McMichael, J. H. Judy, K. Takano, and A. E. Berkowitz, J. Appl. Phys. **82**, 6142 (1997).
[6] C. H. Marrows, B. J. Hickey, M. Malinowska, and C. Mény, IEEE Trans. Magn. **33**, 3673 (1997).
[7] C. H. Marrows and B. J. Hickey, Phys. Rev. B **59**, 463 (1999).
[8] G. Rupp and H. A. M. van den Berg, IEEE Trans. Magn. **29**, 3102 (1993).
[9] B. Heinrich, J. F. Cochran, T. Monchesky, and R. Urban, Phys. Rev. B **59**, 14 520 (1999).
[10] S. M. Rezende, C. Chesman, M. A. Lucena, M. C. de Moura, A. Azevedo, F. M. de Aguiar, and S. S. P. Parkin, J. Appl. Phys. **85**, 5892 (1999).
[11] T. Duden and E. Bauer, Phys. Rev. B **59**, 474 (1999).
[12] H. Yanagihara, K. Pettit, M. B. Salamon, E. Kita, and S. S. P. Parkin, J. Appl. Phys. **81**, 5197 (1999).
[13] Y. Endo, O. Kitakami, and Y. Shimada, Phys. Rev. B **59**, 4279 (1999).
[14] C. C. Yu and A. K. Petford-Long, J. Appl. Phys. **85**, 5753 (1999).
[15] S. O. Demokritov, J. Phys. D **31**, 925 (998).
[16] C. R. Meissner, *Transactions of the 7th National Vacuum Symposium, AVS* (Pergamon Press, London, 1960), p. 196.
[17] http://www.dl.ac.uk/srs/XRD/2.3.dir/
[18] J. N. Chapman, J. Appl. Phys. **17**, 623 (1984).
[19] B. Khamsehpour, C. D. W. Wilkinson, J. N. Chapman, and A. B. Johnston, J. Vac. Sci. Technol. B **14**, 3361 (1996).
[20] C. H. Marrows, Ph.D. thesis, University of Leeds, 1997.
[21] C. C. Kuo, M.-T. Lin, and H. L. Huang, J. Appl. Phys. **85**, 4430 (1999).
[22] C. H. Marrows, N. Wiser, B. J. Hickey, T. P. A. Hase, and B. K. Tanner, J. Phys.: Condens. Matter **11**, 81 (1999).
[23] J. C. Slonczewski, in *Magnetism*, edited by G. T. Rado and H. Suhl (Academic, New York, 1963), Vol. 1, Chap. 5.

[24] M. S. Cohen, E. E. Huber, G. P. Weiss, and D. O. Smith, J. Appl. Phys. **31**, 291S (1960).
[25] R. D. Heidenrich and F. W. Reynolds, in *Structure and Properties of Thin Films*, edited by C. A. Neugebauer, J. B. Newkirk, and D. A. Vermilya (Wiley, New York, 1959), p. 402.
[26] C. H. Marrows, B. J. Hickey, M. Herrmann, S. McVitie, and J. N. Chapman, J. Magn. Magn. Mater. **198**, 408 (1999).
[27] C. H. Marrows and S. Langridge (unpublished).
[28] C. H. Marrows, R. Loloee, and B. J. Hickey, J. Magn. Magn. Mater. **184**, 137 (1998).
[29] C. H. Marrows, F. E. Stanley, and P. W. Mitchell (unpublished).
[30] S. Langridge, J. Schmalian, C. H. Marrows, D. T. Dekadjevi, and B. J. Hickey, cond-mat/9906145 (unpublished).
[31] J.-F. Bobo, H. Fischer, and M. Piecuch, in *Magnetic Ultrathin Films, Multilayers and Surfaces/Interfaces and Characterization*, edited by B. T. Jonker *et al.*, MRS Symposia Proceedings No. 313 (Materials Research Society, Pittsburgh, 1993), p. 467.
[32] J.-F. Bobo, M. Piecuch, and E. Snoek, J. Magn. Magn. Mater. **126**, 440 (1993).
[33] J. C. Slonczewski, Phys. Rev. Lett. **67**, 3172 (1991).
[34] K. Pettit, S. Gider, S. S. P. Parkin, and M. B. Salamon, Phys. Rev. B **56**, 7819 (1997).
[35] J. N. Chapman, J. Rose, P. R. Aitchison, H. Holloway, and D. J. Kubinski, J. Appl. Phys. **86**, 1611 (1999).
[36] R. Miranda, Phys. Scr. **T49**, 579 (1993).
[37] D. Greig, M. J. Hall, C. Hammond, B. J. Hickey, H. P. Ho, M. A. Howson, M. J. Walker, N. Wiser, and D. G. Wright, J. Magn. Magn. Mater. **110**, L239 (1992).
[38] W. F. Egelhoff and M. T. Kief, Phys. Rev. B **45**, 7795 (1992).
[39] See, e.g., Refs. 2 and 22, and further citations therein
[40] R. J. Highmore, W. C. Shih, R. E. Somekh, and J. E. Evetts, J. Magn. Magn. Mater. **116**, 249 (1992).